Available online at www.sciencedirect.com
ScienceDirect
Journal of Photochemistry and Photobiology A: Chemistry 188 (2007) 56–64
Journal of Photochemistry and Photobiology A:Chemistry
www.elsevier.com/locate/jphotochem

UV-Fenton discolouration and mineralization of Orange II over hydroxyl-Fe-pillared bentonite

Jianxin Chen, Lizhong Zhu *

Department of Environmental Science, Zhejiang University, Tianmushan Road, Hangzhou 310028, China

Received 4 June 2006; received in revised form 31 August 2006; accepted 21 November 2006
Available online 24 November 2006

Abstract

An efficient solid catalyst, hydroxyl-Fe-pillared bentonite (H-Fe-P-B), was successfully developed for photo-assisted Fenton reaction. The characteristics of the catalyst were detected by N_2 adsorption/desorption, X-ray fluorescence spectroscopy (XRF), X-ray powder diffraction (XRD), UV–vis absorption spectra (UV–vis) and atom force microscopy (AFM). The catalytic activity of H-Fe-P-B was evaluated in discolouration and mineralization of Orange II in UV-Fenton system. The effects of pH, Orange II concentration, UV light wavelength and temperature on Orange II degradation were studied in detail. It was found that the catalytic activity of H-Fe-P-B for H_2O_2 came from Fe-polycations between bentonite sheets rather than Fe^{3+} or Fe^{2+} in tetrahedral or octahedral sheets of bentonite. As the leaching of iron from the H-Fe-P-B after treatment was negligible, the H-Fe-P-B exhibited a high catalytic activity and good long-term stability in multiple runs in the discolouration and mineralization of Orange II. Because of the strong surface acidity, the H-Fe-P-B acted as not only catalyst but also solid acid in UV-Fenton system, as a result, almost 100% colour removal and 95% TOC removal of 0.2 mM Orange II could be obtained at 40 and 120 min even if the initial pH of solution was as high as 9.0. These results implied that the H-Fe-P-B was a promising catalyst for UV-Fenton system.

Keywords: UV-Fenton; Bentonite; Azo-dye; Hydroxyl radical; Degradation; Wastewater

1. Introduction

Photo-Fenton process, one of the advanced oxidant process (AOPs), has been widely studied as a promising way to treat various organic pollutants in wastewater [1–4]. In this system, the free radicals ($^{\bullet}OH$) are considered as dominant species with the potential ability to oxidize almost all organic contaminants into carbon dioxide and water in aqueous solution.

In homogeneous photo-Fenton system, the catalysts of iron ions are dissolved in water. These homogeneous catalysts are generally very efficient for such reactions, but their removal from the treated water is difficult and costly and the use of metallic salts as catalysts may induce additional pollution [5,6]. Furthermore, the homogeneous photo-Fenton process is suffered from the tight range of pH 2–4 [7,8]. So the use of heterogeneous catalysts would be a good alternative in this system and developing of heterogeneous catalysts for photo-Fenton reaction has received increasing research interest in recent years [4–10].

The ideal heterogeneous catalyst should be cheap, suitable for wide range of pH, as well as has good catalytic activity and low catalyst leaching. During the preparation of heterogeneous catalyst, selection of catalyst support is the most important. At present, different materials including organic materials (such as Nafion and resin) and inorganic materials (such as HY zeolite, C fabrics, silica and clay) are selected as catalyst supports [5–10]. The Fe-pillared clay may be one of promising heterogeneous catalyst for photo-Fenton system because of its unique characteristics, abundance and low cost. For example, Feng et al. [5,11] successfully developed α-Fe_2O_3-pillared bentonite as a heterogeneous catalyst for UV-Fenton by calcining the hydroxyl-Fe-pillared bentonite at 350 °C for 24 h. This catalyst showed high catalytic activity and good long-term stability for Orange II discolouration and mineralization. However, the catalytic activity of α-Fe_2O_3-pillared bentonite in UV-Fenton system was sensitive to the pH of solution. When the pH of solution increased from 3.0 to 6.6, the degradation rate constant of 0.2 mM Orange II decreased from 0.193 to 0.077 min^{-1}

* Corresponding author. Tel.: +86 571 88273733; fax: +86 571 88273450.
E-mail address: zlz@zju.edu.cn (L. Zhu).

1010-6030/$ – see front matter © 2006 Elsevier B.V. All rights reserved.
doi:10.1016/j.jphotochem.2006.11.018

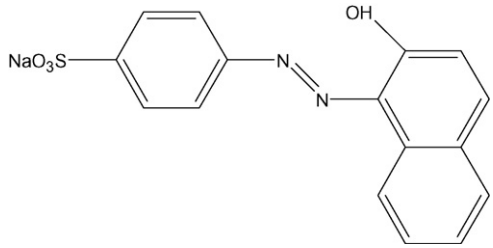

Fig. 1. Chemical structure of Orange II.

and the TOC removal decreased from 100 to about 63% correspondingly [11]. The hydroxyl-Fe-pillared bentonite is another configuration of Fe-pillared bentonite, which is also the precursor of α-Fe_2O_3-pillared bentonite. Without calcinations, the hydroxyl-Fe-pillared bentonite contains mainly Brönsted acid sites [12–14], which may provide additional acid for photo-Fenton. As a result, using this cheaper catalyst may extend the range of pH for photo-Fenton process. Furthermore, discussing the catalytic activity of hydroxyl-Fe-pillared bentonite will be of benefit to understand the structure-property relationships of Fe-pillared bentonite.

The interest of this study is focused on the UV-Fenton process for discolouration and mineralization of azo-dye with hydroxyl-Fe-pillared bentonite as catalyst. The catalytic activity of raw bentonite was also detected to discuss the catalytic ability of different iron configurations in hydroxyl-Fe-pillared bentonite. Orange II was employed as a model compound of azo-dye, which is non-biodegradation and used extensively in textile industry. The results demonstrated that the hydroxyl-Fe-pillared bentonite was an effective and stable catalyst for Orange II discolouration and mineralization in UV-Fenton system. The effects of initial pH, Orange II concentration, reaction temperature and UV wavelength on UV-Fenton process were studied in detail. It was found that the hydroxyl-Fe-pillared bentonite acted as not only catalyst but also solid acid in UV-Fenton system, which led to high colour and TOC removal of Orange II even if the initial pH of solution was as high as 9.0.

2. Experiment

2.1. Materials

The bentonite used was primarily Ca^{2+}-montomorillonite from Inner Mongolia Autonomous Region, China. Its chemical formula was $Ca_{0.39}Na_{0.02}K_{0.02}$ $(Si_{7.91}Al_{0.09})$ $(Al_{2.51}Fe_{0.45}Mg_{1.10})O_{20}(OH)_4nH_2O$ and its cation-exchange capacity (CEC) was 108.4 mM 100 g^{-1}. Bentonite was mechanically grinded with a mortar and pestle to less than 200-mesh (0.074 mm). Orange II purchased from Shanghai Chemical Reagent Company was of chemical reagent grade and used without further purification. And its chemical structure was shown in Fig. 1. H_2O_2 (30% in H_2O), Na_2CO_3, $Fe(NO_3)_3$, Na_2SO_3, KH_2PO_4, KI, NaOH and HCl were of analytical grade and obtained from Shanghai Chemical Reagent Company.

2.2. Synthesis and characterization of hydroxyl-Fe-pillared bentonite

The hydroxyl-Fe-pillared bentonite catalyst was prepared by pillaring the bentonite through cation-exchange process. Firstly, Na_2CO_3 was added slowly as a powder into the solution of $Fe(NO_3)_3$ under magnetic stirring and N_2 atmosphere, until the molar ratio of $[Na^+]/[Fe^{3+}]$ became 1:1. Then the solution was aged at 60 °C for 1 d. Secondly, the intercalant solution was added to the clay suspension under stirring. The final $[Fe^{3+}]$/clay ratio was equal to 10 mol kg^{-1} of dry clay. The product was then filtered, washed with deionized water several times. Then the hydroxyl-Fe-pillared bentonite was dried at 105 °C overnight, ground to less than 200-mesh (0.074 mm).

The d_{001}-spacing was measured by XRD analysis on a D/max-2550 (Rigaku) diffractometer. Specific surfaces area was determined by N_2 adsorption (BET method) on a NOVA2000e instrument. The samples were degassed at 473 K for 3 h before the adsorption and the external and micropore surface area determined with the *t*-plot method. Atom force microscopy (AFM) measurement was performed with SPM-9500J3 (Shimadzu) in the contact mode. The element content of raw bentonite and solid catalyst was analyzed by X-ray fluorescence (XRF) spectrometer (ZSX100e). The UV–vis absorption spectra were measured by UV-2401 (Shimadzu) double-beam digital spectrophotometer equipped with conventional components of a reflectance spectrometer (diffuse reflectance of $BaSO_4$/diffuse reflectance of sample).

2.3. Degradation of azo-dye Orange II

The experiments were carried out in a photocatalytic oxidation reactor, which is consisted of a 4.5 cm diameter quartz tube and 6.0 cm diameter glass column. In the center of the cylindrical reactor, one 6 W UV light tube was used as light resource. The temperature was controlled to 30 °C during the experiments. The dosage of catalyst was 1.0 g L^{-1} and the concentration of H_2O_2 was 10 mM. All experiments were carried out under constantly stirring to make the catalyst good dispersion. Deionized water was used throughout the work. Before reaction, the suspension containing 1.0 g L^{-1} H-Fe-P-B or raw bentonite and Orange II solution was stirred in dark for 1 h to achieve adsorption equilibrium. The reaction was initiated when the UV light was turned on and H_2O_2 was added to the Orange II solution. The pH of the dye solution was measured by using a Mettler Toledo pH meter (Seven multi).

At given intervals of degradation, a sample was analyzed by UV–vis spectroscopy (Shimadzu UV-2450) at a wavelength of 484 nm, which is the maximum absorption wavelength of Orange II [15,16]. The concentration of Orange II was converted through the standard curve method of dyes. Total organic carbon (TOC) was analyzed in a TOC analyzer (Shimadzu TOC-Vcph) to evaluate the mineralization of dyes. Before analysis, all the samples were immediately treated with scavenging reagent (0.1 M Na_2SO_3, 0.1 M KH_2PO_4, 0.1 M KI and 0.05 M NaOH) to obtained accurate TOC values [11]. The

Table 1
The characteristic of bentonite and H-Fe-P-B

Samples	BET surface area ($m^2\ g^{-1}$)			The main element content (wt%)			XRD d_{001} (Å)
	Specific surface area	External surface area	Micropore area	Fe_2O_3	CaO	Al/Si	
Bentonite	55.4	25.2	30.2	4.71	2.75	0.32	15.2
H-Fe-P-B	138.3	43.8	94.5	24.43	0.32	0.31	54.5

organic carbon content (f_{oc}) of catalyst was analyzed in a TOC analyzer (Shimadzu SSM-5000A). To evaluate the stability of the catalyst, the iron concentrations in the solution versus time were determined by atomic absorption (Perkin-Elmer Aanalyst 700). And before analysis, all the samples were immediately filtered through a Millipore filter (pore size 0.22 μm) to remove H-Fe-P-B particles.

3. Results and discussion

3.1. Characterization of H-Fe-B catalyst

The main characteristics of bentonite and H-Fe-P-B are given in Table 1. It can be seen from Table 1 that the BET surface area of bentonite increased remarkably after pillaring. And the inter-

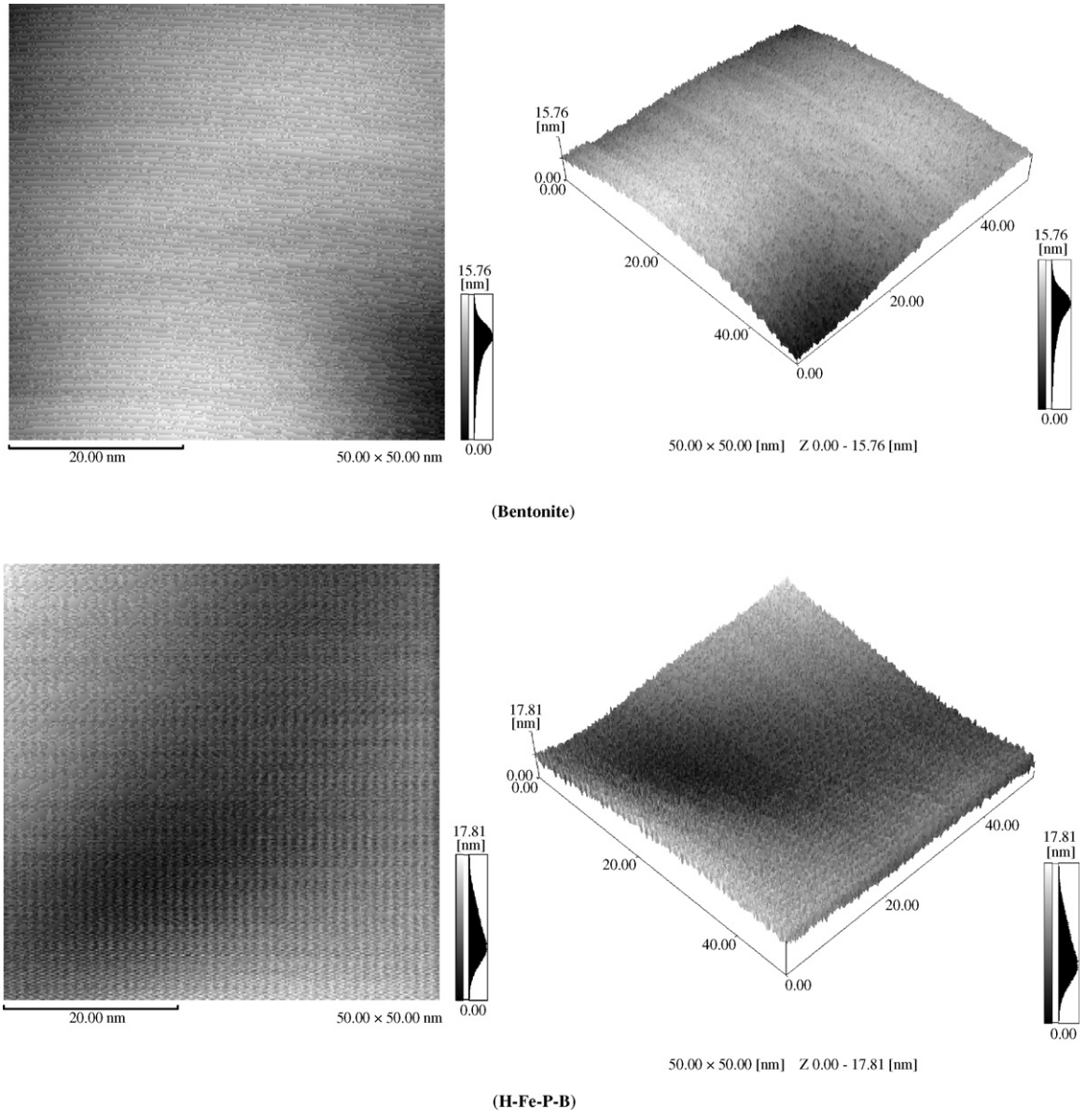

Fig. 2. AFM height and 3D images of the surface of bentonite and H-Fe-P-B.

lamellar distance (d_{001}) of H-Fe-P-B was 5.45 nm while the bentonite was 1.52 nm, which was a criteria interlamellar distance of Ca^{2+}-montomorillonite. These results indicated that the iron ions intercalated the bentonite successfully. The content of iron of H-Fe-P-B reached 17.1%, which was much more than expected from the CEC of the montmorillonite, conforming that the Fe^{3+} was present as polycation (hydroxyl-Fe species). Typical AFM height and 3D images for the bentonite and H-Fe-P-B were shown in Fig. 2. It can be seen that the surface roughness of H-Fe-P-B was higher than that of bentonite, which was in good agreement with their external surface area determined by BET method (shown in Table 1). There are several possible reasons for this phenomenon. One possibility is the Fe-polycations are partly fixed on the surface of bentonite. Another possibility is that surface erosion of Al^{3+} octahedral sheet may occur during the pillaring process, since the ratio of Al/Si of H-Fe-P-B is slightly lower than that of bentonite.

3.2. Catalytic degradation of Orange II by UV-Fenton

There are two different configurations of Fe in the H-Fe-P-B. One is the isomorphous substitution of iron ions for Si^{4+} in the tetrahedral layer or Al^{3+} in the octahedral; the other is presented as hydroxyl-Fe species between bentonite sheets. To detect the catalytic activity of bentonite for hydrogen peroxide, the degradation of Orange II in the presence of bentonite and/or H_2O_2 under UV irradiation or in the dark was studied and the results were shown in Fig. 3. Degradation of Orange II was not observed over 2 h in the presence of H_2O_2 only (curve a) or in the bentonite-H_2O_2 system (curve b). The results suggest that Orange II is stable towards H_2O_2 and the raw bentonite shows no catalytic activity for hydrogen peroxide in dark. The degradation of Orange II was significant and showed pseudo-first-order kinetics for the first 40 min irradiation in UV-H_2O_2 system (the rate constant, k_{obs} is 0.104 min^{-1}) (curve d). The fast decrease in the Orange II concentration is due to the generation of $^{\bullet}OH$ radicals by the direct photolysis of H_2O_2 (Eq. (1)) [3]. In the UV-bentonite-H_2O_2 system (curve c), degradation of Orange II was slightly slower than that in UV-H_2O_2 system, and the rate constant decreased to 0.102 min^{-1}. For the Fenton-like reagent, the initial reactions could be expressed as Eqs. (2)–(9) [17,18]. Under light irradiation or not, an Fe(III)-hydroperoxo intermediate is formed as the first step via hydrolysis with no O–O bond of H_2O_2 broken (Eqs. (2) and (3)). Then the Fe(III)-hydroperoxo may homolyze at the Fe–O bond, producing Fe(II) and $^{\bullet}OOH$ radical (Eq. (4)) or $^{\bullet}OOH^{*}$ radical under irradiation (Eq. (7)). If the Fe(III)-hydroperoxo homolyzes at the O–O bond, the ferryl or highly reactive Fe(V) species will form. The isomorphous substitution of iron ions for Si^{4+} in the tetrahedral layer or Al^{3+} in the octahedral layer block the generation of Fe(III)-hydroperoxo intermediate (Eqs. (2) and (3)). So the iron ions of raw bentonite showed no obvious catalytic activity for hydrogen peroxide.

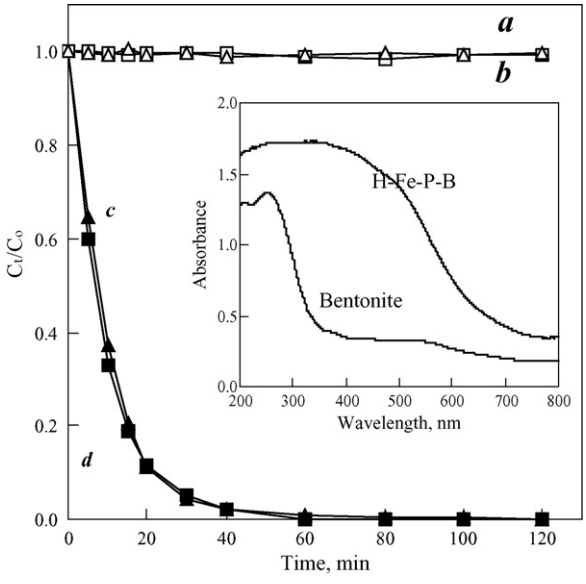

Fig. 3. Degradation of Orange II at an initial solution pH of 3.0 and 30 °C: (a) 10 mM H_2O_2, (b) 1.0 g L^{-1} bentonite + 10 mM H_2O_2, (c) 6 W of UVC + 1.0 g L^{-1} bentonite + 10 mM H_2O_2 and (d) 6 W of UVC + 10 mM H_2O_2. *Inset*: UV–vis absorption spectra of raw bentonite and H-Fe-P-B powders.

$$H_2O_2 + UV \xrightarrow{(\lambda<320\,nm)} {}^{\bullet}OH + {}^{\bullet}OH \quad (1)$$

$$Fe^{3+} + H_2O_2 \rightarrow H^+ + [Fe^{III}OOH]^{2+} \quad (2)$$

$$Fe^{3+} + H_2O_2 \xrightarrow{h\nu} H^+ + [Fe^{III}OOH]^{2+*} \quad (3)$$

$$[Fe^{III}OOH]^{2+} \rightarrow Fe^{2+} + {}^{\bullet}OOH \quad (4)$$

$$[Fe^{III}OOH]^{2+} \rightarrow [Fe^{IV}{=}O]^{2+} + {}^{\bullet}OH \quad (5)$$

$$[Fe^{III}OOH]^{2+} \rightarrow [Fe^{V}{=}O]^{3+} + OH^- \quad (6)$$

$$[Fe^{III}OOH]^{2+*} \rightarrow Fe^{2+} + {}^{\bullet}OOH^{*} \quad (7)$$

$$[Fe^{III}OOH]^{2+*} \rightarrow \{Fe^{III}{-}O \leftrightarrow Fe^{IV}{=}O\}^{2+} + {}^{\bullet}OH \quad (8)$$

$$[Fe^{III}OOH]^{2+*} \rightarrow [Fe^{V}{=}O]^{3+} + OH^- \quad (9)$$

In addition, degradation of Orange II in the UV-bentonite-H_2O_2 system (curve c) is also due to the generation of $^{\bullet}OH$ radicals by the direct photolysis of H_2O_2. As shown in Fig. 3 (inset), the UV–vis spectra of raw bentonite showed a significant absorption in the region 200–330 nm, which means that the efficiency of direct photolysis of H_2O_2 will decrease slightly in the present of bentonite, resulting the slight decrease of Orange II degradation rate.

The discolouration of Orange II in the presence of H-Fe-P-B and/or H_2O_2 under UV irradiation or in the dark versus time was illustrated in Fig. 4A. H_2O_2 and H-Fe-P-B composed a Fenton-like system (curve b). In Fenton-like system, the formation of hydroxyl radical is due to catalytic decomposition of H_2O_2 with Fe^{2+} (Eq. (11)), which is generated by reaction of Fe^{3+} and H_2O_2 (Eq. (10)) [9]. The rate of Eq. (10) is relatively low and the hydroxyl radical generated from the decomposition of H_2O_2 with Fe^{2+} was not enough, so the oxidation of Orange II by hydroxyl radical could not be carried out effectively. When the reaction was carried out in UV-Fenton system (curve d, with H-Fe-P-B and H_2O_2 and UV), the fastest degradation of Orange II was observed and the rate constant increased up to 0.175 min^{-1}. Under UV light irradiation, Fe^{2+} could be formed following Eq.

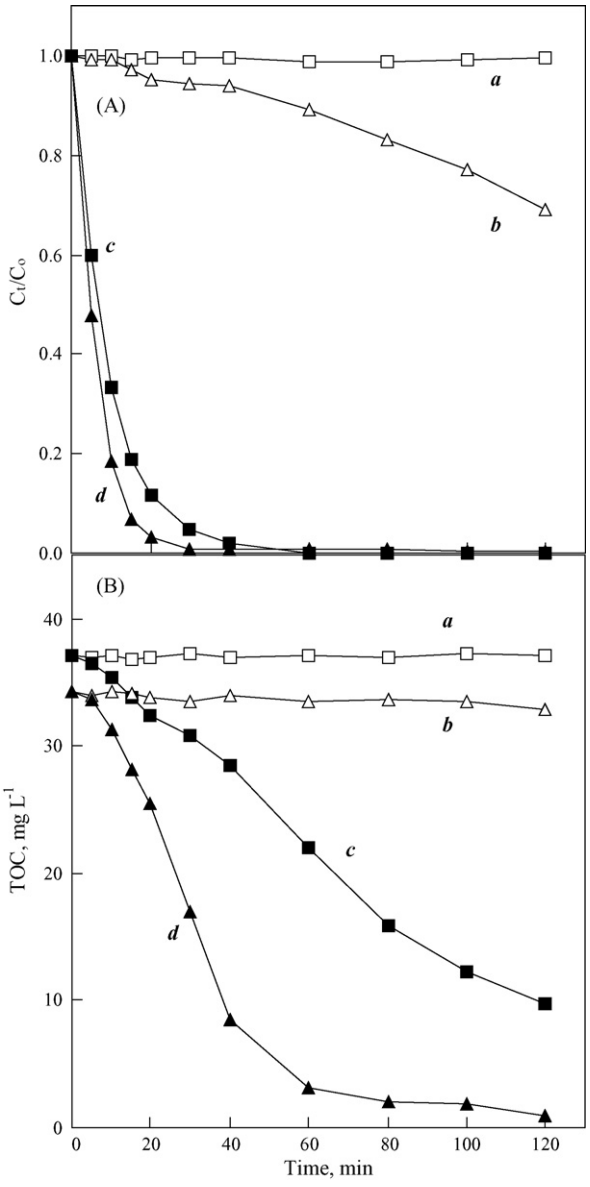

Fig. 4. (A and B) Degradation and mineralization of Orange II at an initial solution pH of 3.0 and 30 °C: (a) 10 mM H_2O_2, (b) 1.0 g L^{-1} H-Fe-P-B + 10 mM H_2O_2, (c) 6 W of UVC + 10 mM H_2O_2 and (d) 6 W of UVC + 1.0 g L^{-1} H-Fe-P-B + 10 mM H_2O_2.

(12) and the enhanced rate of reaction is due to the $^{\bullet}OH$ radical generated from the decomposition of H_2O_2 with Fe^{2+} in photo-Fenton reactions. The results implied that the catalytic activity of H-Fe-P-B for H_2O_2 came from hydroxyl-Fe between sheets rather than Fe^{3+} or Fe^{2+} in tetrahedral or octahedral sheets.

$$Fe^{3+} + H_2O_2 \rightarrow Fe^{2+} + HOO^{\bullet} + H^+, \quad k_1 = 0.02\,M\,s^{-1} \tag{10}$$

$$Fe^{2+} + H_2O_2 \rightarrow Fe^{3+} + {}^{\bullet}OH + OH^-, \quad k_2 = 58\,M\,s^{-1} \tag{11}$$

$$Fe^{III}_{aq} + UV \rightarrow Fe^{2+} + {}^{\bullet}OH \tag{12}$$

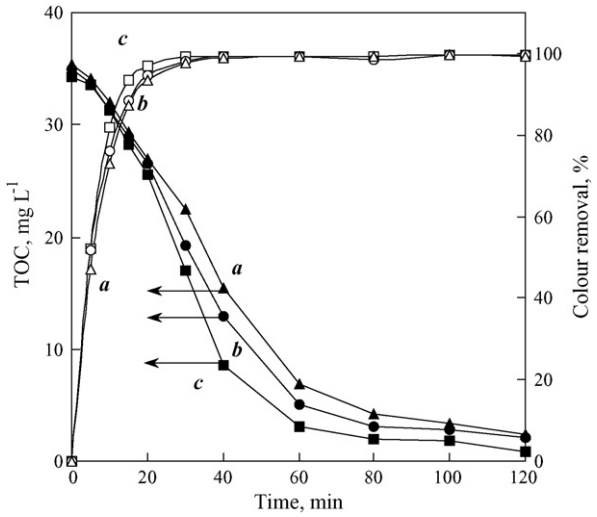

Fig. 5. Effect of pH on degradation and mineralization of Orange II during UV-Fenton process: (a) pH 9.0, (b) pH 6.6 and (c) pH 3.0.

To verify whether Orange II was mineralized or just discoloured, the mineralization of Orange II in solution was quantitatively characterized by TOC analysis. Fig. 4B illustrated the changes of TOC value of the reaction solution versus time under different conditions. From the results, significant decrease of TOC was obtained only in the UV-H_2O_2 (curve c) and UV-Fenton system (curve d) and the TOC removal was much slower than the colour removal. The azo-dye is characterized by nitrogen to nitrogen bond (–N=N–), and the absorption at 484 nm is due to the colour of Orange II solution (n–p^* transition in N=N group). The results indicated that the azo bond of Orange II is more active site for oxidative attack and some colourless intermediates were formed during the degradation of Orange II. Although 100% colour removal efficiency could be obtained at 60 min in the UV-H_2O_2 system, its TOC removal efficiency was only 41%. In UV-Fenton system (curve d), the TOC removals were 92 and 98% after 60 and 120 min irradiation, which means that the UV-Fenton process is a more effective technique than UV-H_2O_2 process for complete mineralization of Orange II.

3.3. Effect of initial pH on degradation of Orange II

The effect of initial pH of solution on discolouration and mineralization of Orange II was presented in Fig. 5. The results showed that the Orange II was degraded and mineralized most efficiently by UV-Fenton at an initial pH of 3.0. As the pH of solution increased from 3.0 to 6.6 to 9.0, the pseudo-first-order kinetic rate constants decreased from 0.175 to 0.138 to 0.129 min^{-1}, respectively. However, almost 100% colour removal and 95% TOC removal could be obtained at 40 and 120 min even if the initial pH of solution was as high as 9.0. This observation is the most important since it is well known that one major drawback of homogeneous photo-Fenton is the tight range of pH for this reaction. And the acidification is more costly than the energy and oxidant used in Fenton degradation [19],

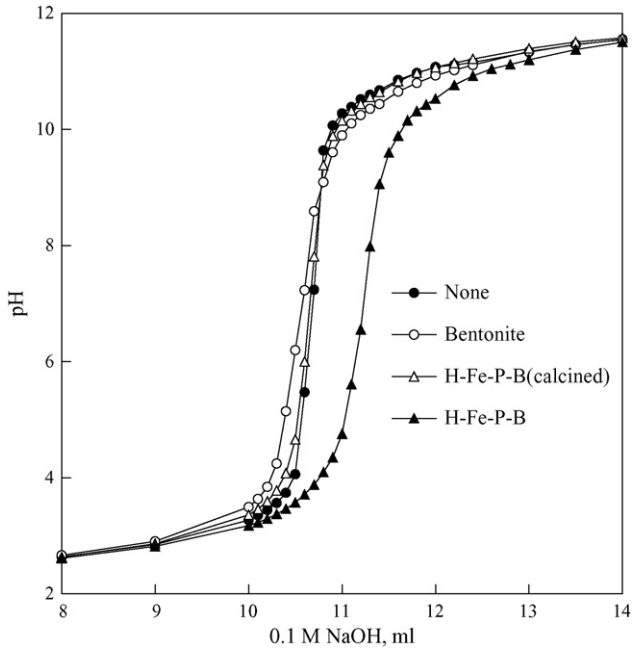

Fig. 6. Titration curves of 1.0 g L^{-1} bentonite and H-Fe-P-B (or calcined) suspended in 100 mL 0.01 M HCl solution with 0.1 M NaOH solution.

which limits its practical industrial application of wastewater treatment.

The phenomenon that the Pillared Clays (PILCs) could extend the range of pH values for Fenton-type oxidation was also reported by Catrinescu et al. [20], who argued that depending on the electronegativity of the pillared bentonite surface, the condensation reaction of iron ions between sheets of bentonite could be prevented or slowed down over a wide range of pH. Moreover, the surface acidity of pillared clay may be another important reason. Pillared clays usually contain Brönsted and Lewis acid sites, which come from the pillars between the bentonite sheets. The H-Fe-P-B contains mainly Brönsted rather than Lewis acid site [12–14]. After calcinations at a high temperature, the hydroxyl-Fe species will be converted to oxide pillars through dehydration and dehydroxylation process and the Brönsted acid sites of pillars will change into Lewis acid sites [12–14].

The acid–base buffering capacities of these materials in water were different (shown in Fig. 6). As to hydroxyl-Fe-pillared bentonite, the Fe-polycations could be expressed as $[Fe_n(OH)_m(H_2O)_x]^{(3n-m)+}$, which are the intermediate derivatives between the primary hydrolyzed products and the insoluble ones (such as $Fe(OH)_3$ or FeOOH) [1,21,22]. In the alkaline aqueous solution, most bases will be consumed by the Fe-polycations in the bentonite interlayer. At the same time, part of hydroxo edge (Fe-OH-Fe) of Fe polycation changed into oxo corner (Fe-O-Fe) (Eq. (13)). As a result, the pH of solution dropped after dark adsorption equilibrium and the degradation of Orange II could occur effectively by UV-Fenton process. This work can also lead to a better understanding of the photochemical activity of Fe-polycation.

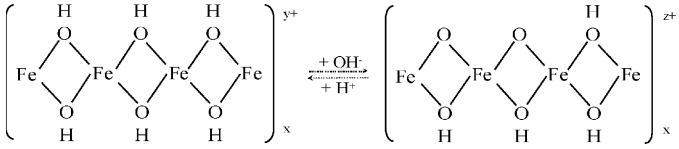

(13)

3.4. Effect of UV light wavelength on degradation of Orange II

The influence of UV light wavelength on the discolouration and mineralization of Orange II in UV-Fenton system was illustrated in Fig. 7. It is obvious that the UV light wavelength can strongly influence the degradation efficiency of Orange II. Both TOC and colour removal efficiency increased when the UV light wavelength decreased. In photo-Fenton reaction, the discolouration and mineralization of dye is due to the •OH radical generated from the decomposition of H_2O_2 with Fe^{2+}. The photoreduction of Fe^{3+} is the most important reaction in the photo-Fenton system, since Fe^{2+} is generated in this step and lead to Fenton reaction. It was reported that the quantum yields of photo-reduction for Fe^{3+} to Fe^{2+} are 0.017, 0.195 and 0.69 at 360, 313 and 254 nm, respectively [2,23,24]. The quantum yield for the photolysis of Fe^{3+} significantly increases as the light wavelength decreases, which leads to increase of colour and TOC removal of Orange II in UV-Fenton system. From the UV–vis spectra of H-Fe-P-B (Fig. 3 (inset)), significant absorption shifted into the visible region and the maximum absorption wavelength of H-Fe-P-B was around 370 nm, belonging to the electrons transition of the Fe–O bond. The results implied that the absorption coefficient of H-Fe-P-B is relatively higher while the photoreduction efficiency of H-Fe-P-B is lower at longer wavelength (365 nm).

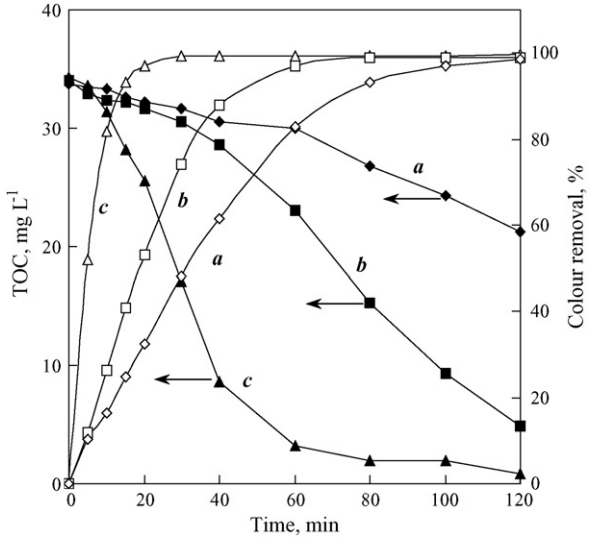

Fig. 7. Effect of UV light wavelength on degradation and mineralization of Orange II during UV-Fenton process: (a) λ = 365 nm, (b) λ = 310 nm and (c) λ = 254 nm.

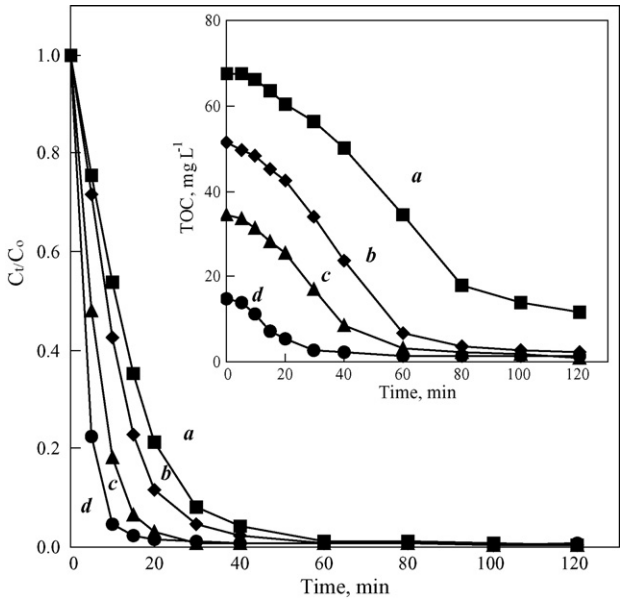

Fig. 8. Effect of initial concentration of Orange II on degradation and mineralization of Orange II during UV-Fenton process: (a) 0.1 mM, (b) 0.2 mM, (c) 0.3 mM and (d) 0.4 mM.

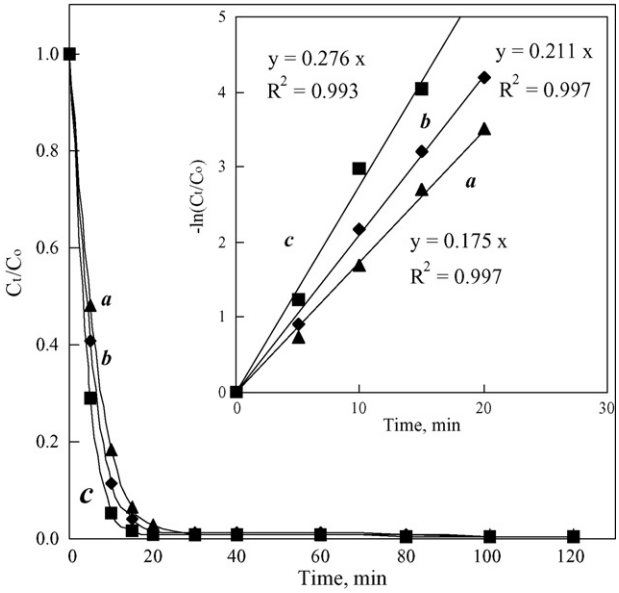

Fig. 9. Effect of temperature on degradation of Orange II during UV-Fenton process: (a) 30 °C, (b) 40 °C and (c) 50 °C. *Inset*: Determination of pseudo-first-order rate constants for Orange II degradation under different conditions.

3.5. Effect of initial Orange II concentration on its degradation

The effect of initial concentrations of Orange II on its degradation in UV-Fenton system was depicted in Fig. 8. Based on the data presented in Fig. 8, the rate constants and initial rates at different Orange II concentrations were calculated and summarized in Table 2. On the one hand, Orange II in solution can strongly absorb UV light at 254 nm derived from aromatic rings [16], so the intensity of UV light decreased with the increase of Orange II concentration and the •OH radical yield decreased consequently. As the initial concentration of Orange II increased from 0.1 to 0.4 mM, the value of k_{obs} decreased from 0.303 to 0.078 min^{-1}. On the other hand, the adsorption of Orange II onto the catalyst can facilitate the degradation of the dye by UV-Fenton process. As a result, the initial rate of Orange II degradation varied slightly with the increase of Orange II concentration, and a peak value of 0.350 M min^{-1} is presented at 0.2 mM Orange II.

The TOC values of Orange II solution as a function of reaction time at different Orange II concentrations were depicted in Fig. 8 (inset). The results showed that the Orange II could be mineralized effectively by UV-Fenton system, even if the initial concentration of the dye is as high as 0.4 mM. The mineralization of Orange II by H_2O_2 could be written as Eq. (14) [24]. According to this chemical formula, when the initial concentration of Orange II was 0.4 mM, the theoretically concentration of H_2O_2 should be 16.8 mM. In this experiment, the concentration of H_2O_2 was 10 mM, which was lower than the theoretical value, so the residual TOC of solution with a higher initial concentration (0.4 mM) reached 11.8 mg L^{-1} after 120 min treatment.

$$C_{16}H_{11}N_2NaO_4S + 42H_2O_2 \rightarrow 16CO_2 + 42H_2O + 2HNO_3 + NaHSO_4 \quad (14)$$

3.6. Effect of reaction temperature on degradation of Orange II

The effect of temperature on degradation of Orange II was studied and the results were shown in Fig. 9. Based on the pseudo-first-order equation, the rate constants (k_{obs}) could be obtained by plotting $-\ln(C_t/C_o)$ as a function of time t, and the results were shown in Fig. 9 (inset). It is clear that the value of rate constant was positive relative to the temperature of reaction solution. According to Arrhenius equation, the

Table 2
The pseudo-first-order rate constants and initial rates under different conditions

	UV-H_2O_2	UV-bentonite-H_2O_2	UV-Fenton (initial Orange II concentration)			
			0.1 mM	0.2 mM	0.3 mM	0.4 mM
k_{obs} (min^{-1})	0.104	0.102	0.303	0.175	0.102	0.078
R^2	0.994	0.995	1.000	0.997	0.989	0.990
Initial rate (M min^{-1})	0.021	0.020	0.030	0.035	0.031	0.031

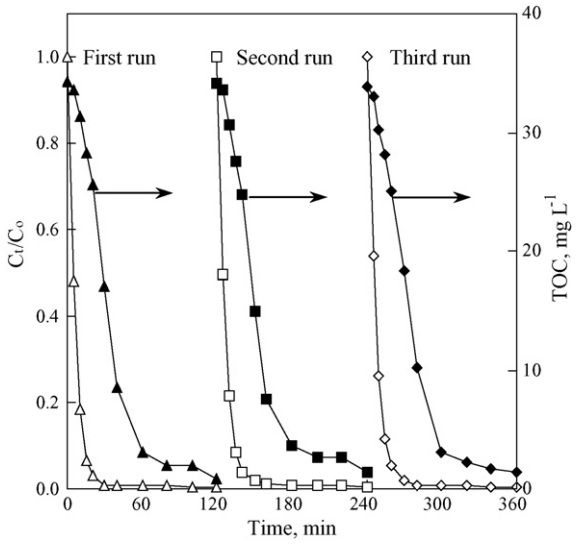

Fig. 10. Degradation and mineralization of Orange II during UV-Fenton process as a function of time up to the third cycle.

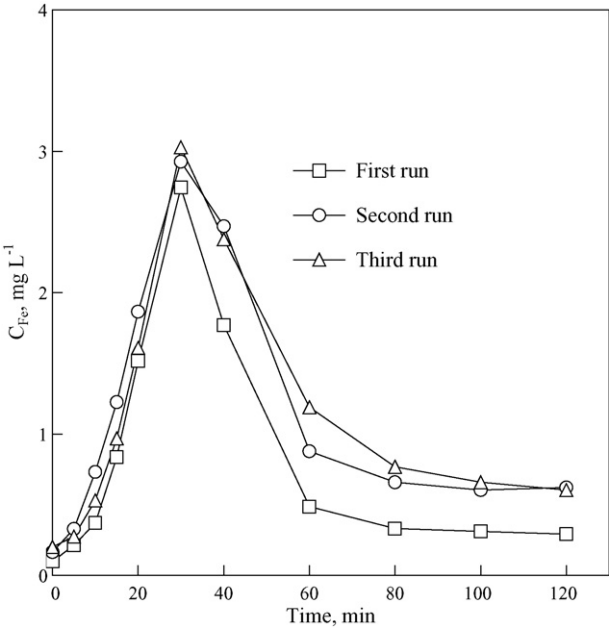

Fig. 11. Concentration of Fe ions in solution during the degradation of Orange II as a function of time up to the third cycle.

reaction activation energy could be calculated, and the value is 18.6 kJ mol^{-1}. The result implied that some activation energy is required during the oxidation of Orange II in UV-Fenton process, although this value is smaller than that of ordinary thermal reactions.

3.7. The stability of H-Fe-P-B catalyst

Stability is an important property for effective catalyst. Fig. 10 illustrated the repetitive Orange II discolouration and mineralization in 120 min cycles. After each recycling, the catalyst was treated by centrifugation, dried and reused. Compared with the results displayed in Fig. 10, it could be found that the kinetics and efficiency of the Orange II degradation varied slightly. The organic carbon content (f_{oc}) of catalyst was analyzed before use (or reuse) and the values were 0.3, 2.0 and 1.9 mg g^{-1}, respectively. The slight difference in the Orange II degradation may due to the sorption of organic intermediates on the catalyst.

Fe ions significantly leached out from the catalyst will lead to decrease of catalytic activity as well as additional metal ions pollution. To detect the Fe leaching from the H-Fe-P-B, the concentrations of iron ions versus time in solution were measured by atomic absorption in each recycling as shown in Fig. 11. After 1 h dark adsorption experiments, the concentrations of Fe were 0.1, 0.2 and 0.2 mg L^{-1} at the start of light experiment, conforming that the catalyst is very stable. During the degradation of Orange II, the iron ions concentration increased firstly and reached peak values (around 3.0 mg L^{-1}) at about 30 min, then decreased to around 0.6 mg L^{-1} after 120 min reaction. According to the EEC regulations, the iron concentrations in wastewater and drinking water must not exceed 5 and 2 mg L^{-1}, respectively [6,25]. The additional environmental pollution could be avoided by using this catalyst in the UV-Fenton system. These results imply that the catalyst has a good long-term stability and activity.

4. Conclusions

Hydroxyl-Fe-pillared bentonite was successfully developed as a catalyst for UV-Fenton discolouration and mineralization of azo-dye. The catalyst was characterized by N_2 adsorption/desorption, XRF, XRD, UV–vis and AFM. The results showed that the BET surface area, interlamellar distance (d_{001}) and iron content of H-Fe-P-B increased remarkably compared with raw bentonite. The H-Fe-P-B exhibited a good long-term stability and high catalytic activity in discolouration and mineralization of Orange II. And the catalytic activity of H-Fe-P-B for H_2O_2 came from Fe-polycation between bentonite sheets rather than Fe^{3+} or Fe^{2+} in tetrahedral or octahedral sheets of bentonite. The Orange II concentration, UV light wavelength and temperature were the main factors that influence the degradation of Orange II during the UV-Fenton process. It was found that the range of pH for UV-Fenton could be extended up to 9.0 by using H-Fe-P-B as catalyst. Under this condition, almost 100% colour removal and 95% TOC removal of 0.2 mM Orange II could be achieved after 40 and 120 min irradiation.

Acknowledgements

This work was supported by grants from the National Natural Science Foundation of China (50378081) and the State 863 High Technology R&D Project of China (2002AA302305).

References

[1] L. Garrel, M. Bonetti, L. Tonucci, N. d'Alessandro, M. Bressan, J. Photochem. Photobiol. A: Chem. 179 (2006) 193.
[2] C. Lee, J. Yoon, Chemosphere 57 (2004) 1449.
[3] F. Herrera, J. Kiwi, A. Lopez, V. Nadtochenko, Environ. Sci. Technol. 33 (1999) 3145.

[4] J. He, W. Ma, J. He, J. Zhao, J.C. Yu, Appl. Catal. B: Environ. 39 (2002) 211.
[5] J. Feng, X. Hu, P.L. Yue, Environ. Sci. Technol. 38 (2004) 269.
[6] A. Bozzi, T. Yuranova, J. Mielczarski, J. Kiwi, New. J. Chem. 28 (2004) 519.
[7] M. Noorjahan, V. Durga Kumari, M. Subrahmanyam, L. Panda, Appl. Catal. B: Environ. 57 (2005) 291.
[8] S. Parra, I. Guasaquillo, O. Enea, E. Mielczarski, J. Mielczarki, P. Albers, L. Kiwi-Minsker, J. Kiwi, J. Phys. Chem. B 107 (2003) 7026.
[9] M. Cheng, W. Ma, J. Li, Y. Huang, J. Zhao, Y.X. Wen, Y. Xu, Environ. Sci. Technol. 38 (2004) 1569.
[10] A. Bozzi, T. Yuranova, P. Lais, J. Kiwi, Water Res. 39 (2005) 1441.
[11] J. Feng, X. Hu, P.L. Yue, Environ. Sci. Technol. 38 (2004) 5773.
[12] J.T. Kloprogge, J. Porous Mat. 5 (1998) 5.
[13] F. Kooli, W. Jones, Chem. Mater. 9 (1997) 2913.
[14] Y.S. Han, S. Yamanaka, J.H. Choy, J. State Chem. 144 (1999) 45.
[15] F. Chen, W. Ma, J. He, J. Zhao, J. Phys. Chem. A 106 (2002) 9485.
[16] Y. Mu, H.Q. Yu, J.C. Zheng, S.J. Zhang, J. Photochem. Photobiol. A: Chem. 163 (2004) 311.
[17] J.J. Pignatello, D. Liu, P. Huston, Environ. Sci. Technol. 33 (1999) 1832.
[18] B. Ensing, F. Buda, E.J. Baerends, J. Phys. Chem. A 107 (2003) 5722.
[19] D. Gumy, P. Fernández-Ibáñez, S. Malato, C. Pulgarin, O. Enea, J. Kiwi, Catal. Today 101 (2005) 375.
[20] C. Catrinescu, C. Teodosiu, M. Macoveanu, J. Miehe-Brendlé, R. Le Dred, Water Res. 37 (2003) 1154.
[21] J.Y. Bottero, A. Manceau, F. Villieras, D. Tchoubar, Langmuir 10 (1994) 316.
[22] C.M. Flynn, Chem. Rev. 84 (1984) 31.
[23] D.R. de Souza, E.T.F. Mendonça Duarte, G. de Souza Girardi, V. Velani, A.E. da Hora Machado, C. Sattler, L. de Oliveira, J.A. de Miranda, J. Photochem. Photobiol. A: Chem. 179 (2006) 269.
[24] J. Feng, X. Hu, P.L. Yue, H.Y. Zhu, G.Q. Lu, Ind. Eng. Chem. Res. 42 (2003) 2058.
[25] V. Lenoble, C. Laclautre, V. Deluchat, B. Serpaud, J.C. Bollinger, J. Hazard. Mater. B 123 (2005) 262.